# Suspended heated silicon platform for rapid thermal control of surface reactions with application to carbon nanotube synthesis

Lucas van Laake, Anastasios John Hart,[a] and Alexander H. Slocum
*Department of Mechanical Engineering, Massachusetts Institute of Technology, 77 Massachusetts Avenue, Room 3-470, Cambridge, Massachusetts 02139*

(Received 14 December 2006; accepted 26 June 2007; published online 3 August 2007)

Rapid continuous thermal control of chemical reactions such as those for chemical vapor deposition (CVD) growth of nanotubes and nanowires cannot be studied using traditional reactors such as tube furnaces, which have large thermal masses. We present the design, modeling, and verification of a simple, low-cost reactor based on resistive heating of a suspended silicon platform. This system achieves slew rates exceeding 100 °C/s, enabling studies of rapid heating and thermal cycling. Moreover, the reaction surface is available for optical monitoring. A first-generation CVD apparatus encapsulates the heated silicon platform inside a sealed quartz tube, and initial experiments demonstrate growth of films of tangled single-wall and aligned multiwall carbon nanotubes using this system. The reactor can be straightforwardly scaled to larger or smaller substrate sizes and may be extended for a wide variety of reactions, for performing *in situ* reaction diagnostics, for chip-scale growth of nanostructures, and for rapid thermal processing of microelectronic and micromechanical devices. © *2007 American Institute of Physics.* [DOI: 10.1063/1.2760936]

## I. INTRODUCTION

Studies involving rapid heating and thermal cycling have recently shown that temperature magnitude and its temporal variation can influence the progress of chemical reactions. For example, a 40% increase in the conversion rate of the oxidation of CO was reported under fast forced temperature oscillations,[1] and formation of single-wall carbon nanotubes occurred only under rapid heating[2] of a supported catalyst powder. Although the effects of unsteady conditions have been widely studied for other parameters such as reactant composition, rapid thermal control cannot be studied using traditional reactors due to their large thermal mass.[3]

Many high-temperature gas-phase reactions such as chemical vapor deposition (CVD) processes utilize tube furnaces, where the reaction sample (e.g., a substrate coated with a catalyst) is sealed inside a ceramic (e.g., quartz) tube, and the reactant atmosphere flows through the tube. A laboratory-scale tube furnace which uses resistively heated coils surrounding the tube is typically limited to a heating rate of ~10 °C/min. Effects of rapid heating using tube furnaces have thus been studied by moving the sample or tube with respect to the heater coils[4] or by injecting floating catalyst particles into the heated zone.[2] Alternatively, electrically conductive substrates and/or particles can be directly heated inductively[5] or using microwave radiation.[6,7] However, continuous temperature control of the reaction surface is not routinely achieved by these methods. Some hot stages for atomic force microscopy (AFM) achieve rapid thermal control, but the maximum temperature is limited to 200 °C.[8,9] Further, in traditional CVD setups, the substrate temperature is not directly measured and is rather assumed to be equal to the temperature measured by a thermocouple outside the tube.

Alternatively, microscale chemical reactors exhibit low thermal mass and therefore can achieve more rapid heating and cooling rates than tube furnaces.[1,10] Reactors which contain the flow in microfabricated channels offer high surface-to-volume ratios and are especially fit for reactions where both reactants and products are fluids or gases. However, channels are typically formed by etching and consecutive permanent bonding of substrates, leaving internal surfaces inaccessible for direct deposition of catalyst material or for extraction of deposited material, and limiting access for *in situ* optical monitoring of the reaction.

We present a simple and low-cost heater apparatus that is realized without microfabrication techniques, yet achieves heating and cooling rates equal to or better than existing microchemical systems, and maintains a flow regime comparable to that in a regular tube furnace. This apparatus is designed and tested for studies of carbon nanotube (CNT) growth and could be used for many other surface-bound high-temperature reactions. Further, its principle of operation—resistive heating of a suspended silicon beam contacted by self-cooled electrodes—could be extended for temperature control of microsystems and microreactors. It enables studies of the influence of rapid temperature variation on surface reactions, including rapid initial heating, thermal cycling, and rapid cooling. Further, unlike in a tube furnace, thermal pretreatment of the gas is decoupled from substrate heating; and importantly, there is a clear view of the reaction surface, which allows direct optical monitoring of the reaction progress.

This article presents the design, modeling, and verifica-

[a]Author to whom correspondence should be addressed. Present address: Department of Mechanical Engineering, University of Michigan, Ann Arbor, MI 48109; electronic mail: ajohnh@umich.edu

 © 2007 American Institute of Physics

**Downloaded 03 Aug 2007 to 18.33.7.72. Redistribution subject to AIP license or copyright, see http://rsi.aip.org/rsi/copyright.jsp**

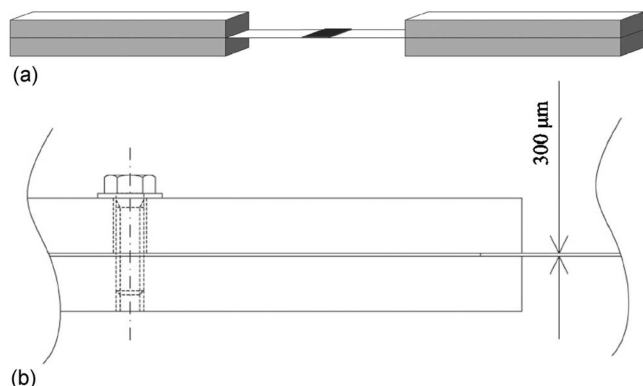


FIG. 1. Design of heated platform and steel electrodes. (a) Schematic representation of "indirect heating" mode. Catalyst may be deposited directly onto the suspended platform ("direct heating"), or a second substrate may be placed on top of the heated substrate. (indirect heating). (b) Detail showing clamping of heated platform (front view, to scale).

tion of the suspended platform heater, along with a first-generation CVD apparatus which encapsulates the heater, and initial results of CNT film growth experiments using the CVD apparatus. Carbon nanotubes are long molecules having exceptional mechanical, thermal, and electrical properties, and these characteristics are generating wide application interest[11,12] along with a need for efficient and rapid manufacturing of CNTs. Simple "desktop" growth of CNT films on the heated platform, improved CNT yield enabled by local heating of the reactant atmosphere, as well as optical observation of the film growth demonstrate additional benefits of our apparatus.

## II. DESIGN AND MODELING OF SUSPENDED PLATFORM HEATER

The design challenge is to enable rapid heating and cooling of a substrate for growth of a CNT film, in a hydrocarbon gas environment, where the substrate surface is maintained at up to 850 °C. The substrate is a segment of a silicon wafer coated with a film of supported metal catalyst deposited by electron beam evaporation. The atmosphere is a varied mixture of $C_2H_4$ (carbon source), $H_2$, and Ar at a total flow rate of less than 1000 SCCM (SCCM denotes cubic centimeter per minute at STP). We have used this combination of catalyst and reactants to grow films of tangled single-wall CNTs and millimeter-tall structures of aligned multiwall CNT nanotubes, using an atmospheric-pressure tube furnace.[13,14]

### A. Heater design

Versus alternatives such as convective, laser, and electromagnetic induction heating,[5] resistive heating is selected for its proven effectiveness in traditional systems and for its simplicity of manufacturing and operation. The key to applying this standard method for rapid heating and cooling is to use a suspended heater element (Fig. 1). This minimizes thermal mass, thus decreasing the input power needed for given slew rate of heating as well as the time constant for cooling. The suspended resistive element ("heated platform") is cleaved from a highly doped silicon wafer (300 $\mu$m thick, 150 mm diameter, $N_A > 10^{18}$, Silicon Quest International). The platform is clamped between stainless steel (AISI 304) blocks, which serve as mechanical anchors and electrical contacts and are allowed to move freely in response to thermal expansion. The contacts act as heat sinks to the platform and remain below 500 °C without active cooling.

In one mode of operation, a silicon substrate ($\approx$10 mm $\times$ 10 mm $\times$ 600 $\mu$m thickness) coated with the catalyst film for CNT growth is rested on the heated platform. Here, the optical flatness of the silicon platform and growth substrate ensure good thermal contact, and there is only a slight ($\approx$10 °C) temperature drop between the platform surface and the top surface of the substrate. Alternatively, the heated platform itself can be coated with catalyst and serve directly as the growth substrate.

The resistivity of silicon is much higher than that of steel ($>1 \times 10^{-4}$ vs $<1 \times 10^{-6}$ $\Omega$ m for the relevant temperature range), resulting in selective heating of the silicon platform; yet the resistivity of silicon is low enough to induce significant heating at limited voltage ($<$50 V). Also, silicon is thermally stable above 850 °C, as long as the substrate is not mechanically stressed which would cause creep. Last, resistivity decreases sharply with temperature above the intrinsic temperature, which results in stable operation when a current source is used. This is illustrated in Fig. 2, which shows a simplified lumped-mass approximation to the dynamics of the system, where the suspended substrate is assumed to have uniform temperature. The heat source is Ohmic dissipation equal to $I^2R$ [Fig. 2(a)] or $V^2/R$ [Fig. 2(b)] and heat loss is limited to radiation and convection. This plot of the temperature change rate ($dT/dt$) as function of temperature for different values of $V$ and $I$ reveals stable and unstable equilibria; a zero indicates an equilibrium point, which is stable if $dT/dt$ is decreasing and unstable if $dT/dt$ is increasing. It is clear that for constant current (a simple laboratory supply in current limited mode) only stable equilibria arise, whereas for constant voltage there are stable equilibria at low temperature and low voltage, but at high temperature or voltage destructive thermal runaway will occur.

### B. Thermal model

A detailed model was created to investigate the thermal response of the silicon heater, as well as to verify the design of the self-cooling contact blocks. Assuming symmetry about the center of the substrate, there are two domains: the steel block (index SB) and half of the heater (HH). Both domains can be described by a Partial differential equation (PDE) of the same form, where the contact between the domains is expressed in the boundary conditions. The resulting coupled PDEs are made nondimensional by appropriate scaling, and the system is solved numerically using the MATLAB™ function PDEPE.m. The model makes the assumptions listed below.

- The system is one dimensional; therefore, the platform temperature is constant over its cross section.
- The system is symmetric about the center of the platform.
- The steel electrodes have zero electrical resistivity.
- There is constant thermal resistance between the steel electrodes and the silicon platform.

Downloaded 03 Aug 2007 to 18.33.7.72. Redistribution subject to AIP license or copyright, see http://rsi.aip.org/rsi/copyright.jsp

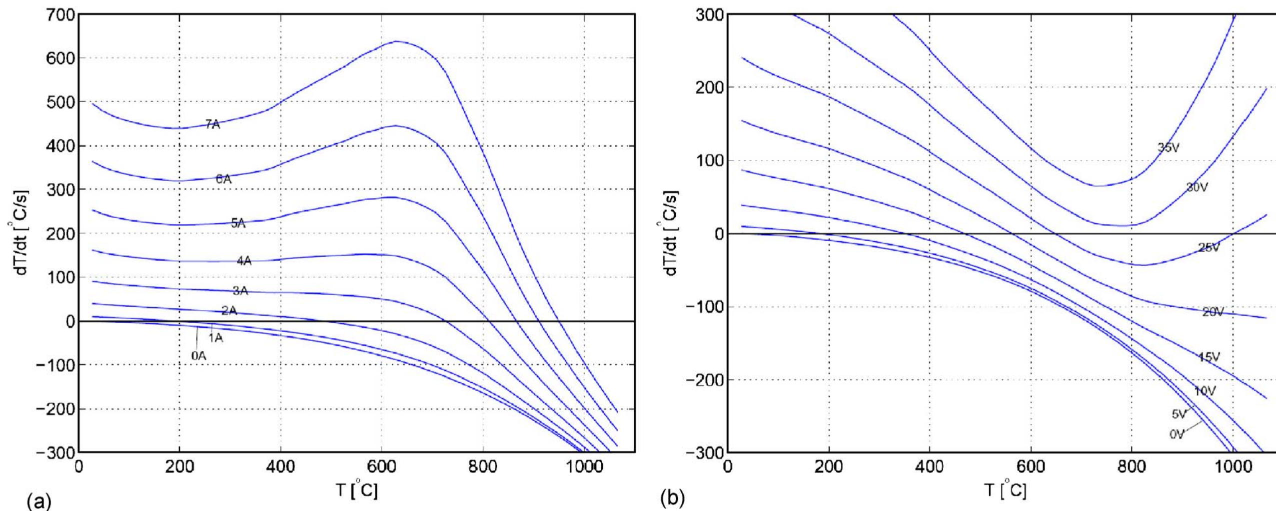


FIG. 2. (Color online) Rate of temperature change vs temperature for a lumped model of a $85\times10\times0.3$ mm$^3$ suspended heater element. (a) Constant current operation, where all equilibrium points are stable. (b) Constant voltage operation, where some equilibrium points are stable, and where no equilibrium points exist for $V>29$ V.

- The surrounding atmosphere circulates sufficiently to maintain a constant ambient temperature.
- The electrical resistivity of silicon is approximated by the bulk value for thermal equilibrium, meaning that thermoelectric effects like the Thomson effect are neglected, and the electric field does not create excess carriers.[15]
- Appropriate temperature-dependent physical properties for silicon and steel are as supplied by the literature.[16,17]

One advantage of the analytical modeling approach is the availability of performance parameters which result from making the model dimensionless. These factors provide insight to the dynamics of the system; for example, time constants predict the heating and cooling responses of the system. Also, simulation of the system response to a highly dynamic input current is straightforward, as the coupled electrical and thermal physics are captured in a single formula. However, with complex geometries where transverse temperature gradients cannot be neglected, two-or three-dimensional models must be constructed. In these cases, a finite element approach would likely prove more effective.

To build the analytical model of our system, conservation of energy is first applied to an element having a constant cross section, as depicted in Fig. 3. In integral form,[18]

$$\varrho C\frac{\partial u}{\partial t} = k\frac{\partial^2 u}{\partial x^2} + Q - \frac{P}{A}w. \tag{1}$$

From left to right, the terms represent heat storage (temperature change), diffusion (conduction), heat dissipation (the resistive heating source), and heat loss to surroundings (through convection and radiation). The resistive heating source $Q$ in the heater (where $Q=0$ in the steel block) and heat loss to the surroundings $w$ (for both domains) are further specified as

$$Q = I^2\left(\frac{\rho}{A^2}\right), \tag{2}$$

$$w = h(u-u_\infty) + \sigma\epsilon(u^4 - u_\infty^4). \tag{3}$$

Boundary conditions [Eqs. (4)–(7)] are applied to represent the following conditions: heat loss at the end of the steel block by convection and radiation,

$$x=0 \rightarrow -\phi = h(u-u_\infty) + \sigma\epsilon(u^4 - u_\infty^4); \tag{4}$$

thermal contact resistance at the interface, where $X_{\mathrm{SB}}^-$ and $X_{\mathrm{SB}}^+$ represent the contact on the side of the steel block and the heater, respectively,

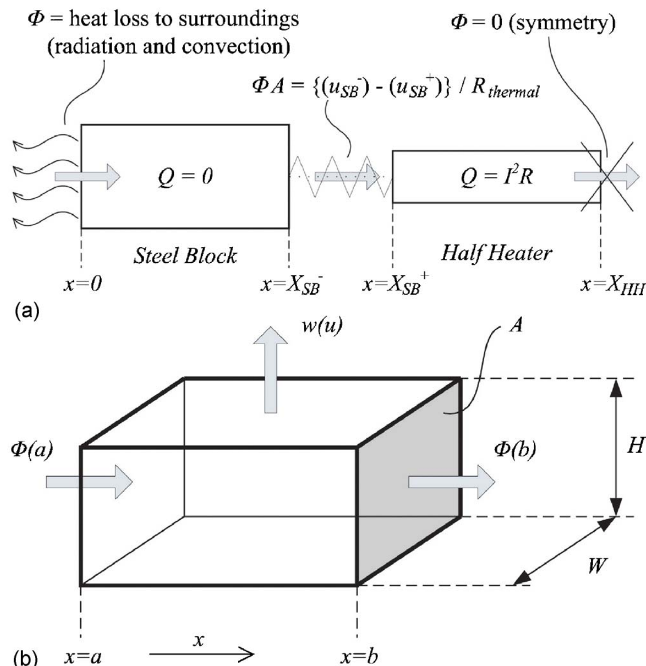


FIG. 3. (Color online) Thermal model. (a) The thermal model describes two domains having different temperature-dependent material properties. Symmetry is translated to a boundary condition of no heat flux in the center of the heater. The connection between a steel electrode and the heater is modeled as a constant thermal contact resistance. (b) Definition of an element on which an integral form of the energy-conservation equation is applied.

Downloaded 03 Aug 2007 to 18.33.7.72. Redistribution subject to AIP license or copyright, see http://rsi.aip.org/rsi/copyright.jsp

$$x = X_{\mathrm{SB}}^- \rightarrow \frac{u_{\mathrm{SB}}^- - u_{\mathrm{SB}}^+}{R_{\mathrm{thermal}}} = \phi A_{\mathrm{SB}}, \tag{5}$$

$$x = X_{\mathrm{SB}}^+ \rightarrow \frac{u_{\mathrm{SB}}^- - u_{\mathrm{SB}}^+}{R_{\mathrm{thermal}}} = \phi A_{\mathrm{HH}}; \tag{6}$$

and symmetry about the center of the heater,

$$x = X_{\mathrm{HH}} \rightarrow \phi = 0. \tag{7}$$

Then the equations are made nondimensional by appropriate scaling. Temperature $u$ is scaled to the temperature of the surroundings such that

$$\tilde{u}_i = \frac{u_i - u_\infty}{u_\infty} \quad (i = \mathrm{SB}, \mathrm{HH}). \tag{8}$$

Position $x$ is scaled according to the lengths of the respective domains dsuch that $\tilde{x}_{\mathrm{SB}}, \tilde{x}_{\mathrm{HH}} \in [0,1]$. This permits solving the problem using the MATLAB™ function PDEPE.m, which can only solve multiple PDEs in parallel if they are on a common spatial grid. Considering this dthe scaled dimensions $\tilde{x}_{\mathrm{SB}}$ and $\tilde{x}_{\mathrm{HH}}$ are chosen in opposing directions in real space; the contact between the steel block dthe silicon heater exists at the same point in scaled space $\tilde{x}_{\mathrm{SB}} = \tilde{x}_{\mathrm{HH}} = 1$, which makes grid refinement around the contact more efficient. The scaled position vectors are

$$\tilde{x}_i = \frac{x - x_{\min}}{x_{\max} - x_{\min}} \Rightarrow \tilde{x}_{\mathrm{SB}} = \frac{x}{X_{\mathrm{SB}}}, \quad \tilde{x}_{\mathrm{HH}} = \frac{X_{\mathrm{HH}} - x}{X_{\mathrm{HH}} - X_{\mathrm{SB}}}. \tag{9}$$

Time is scaled by dividing by an overall time constant,

$$\tilde{t} = \frac{t}{\tau_o}, \tag{10}$$

where $\tau_o$ can be chosen arbitrarily. We take

$$\tau_o = \tau_{c,\mathrm{HH}} // \tau_{r,\mathrm{HH}} // [\tau_{d,\mathrm{HH}} + \tau_{d,\mathrm{SB}} + (\tau_{c,\mathrm{SB}} // \tau_{r,\mathrm{SB}})], \tag{11}$$

where // is defined by

$$\tau_x // \tau_y \equiv (\tau_x^{-1} + \tau_y^{-1})^{-1}. \tag{12}$$

This captures the lumped-mass dynamics of the system during cooling: heat flows mainly from the suspended platform to the surroundings by radiation and convection, in parallel with conduction to the steel blocks and consecutive radiation and convection to the surroundings from there. Time constants for heat loss by diffusion $\tau_d$ [Eq. (14)], convection $\tau_c$ [Eq. (15)], and radiation $\tau_r$ [Eq. (16)] are defined as the product of the thermal mass of domain $i$ (where $i$ indicates steel block or half heater) and the resistance for heat loss $R_{j,i}$ of that domain by diffusion ($R_{d,i}$), convection ($R_{c,i}$), and radiation ($R_{r,i}$), respectively:

$$\tau_{j,i} = (\varrho CV)_i R_{j,i}, \quad (i = \mathrm{SB}, \mathrm{HH}), \tag{13}$$

where

$$R_{d,i} = \left(\frac{L}{kA}\right)_i \Rightarrow \tau_{d,i} = \left(\varrho CV \frac{L}{kA}\right)_i, \tag{14}$$

$$R_{c,i} = \left(\frac{1}{hS}\right)_i \Rightarrow \tau_{c,i} = \left(\varrho CV \frac{1}{hS}\right)_i, \tag{15}$$

and

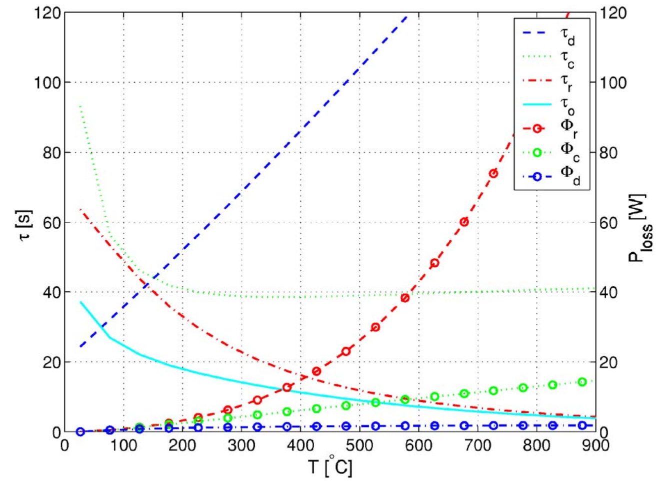


FIG. 4. (Color online) Time constants and heat flow rates as function of temperature for a $85 \times 10 \times 0.3$ mm$^3$ suspended heater element.

$$R_{r,i} = \left\{ \frac{\tilde{u}}{\sigma \epsilon u_\infty^3 S[(\tilde{u}+1)^4 - 1]} \right\}_i \Rightarrow \tau_{r,i} = \left\{ \varrho CV \frac{\tilde{u}}{\sigma \epsilon u_\infty^3 S[(\tilde{u}+1)^4 - 1]} \right\}_i. \tag{16}$$

The physical interpretation of the time constants is especially meaningful for cooling of the silicon element. High heating rates can in principle be achieved by applying a high current, but cooling depends on heat loss. The definition of the time constants as a product of thermal mass and thermal resistance can be interpreted as the energy loss needed for a temperature decrease of one degree divided by the energy that is lost per second and per degree temperature difference by a certain mechanism: radiation, convection, or conduction. This represents the time it takes to lose the stored energy at the current temperature difference, i.e., the time it takes to cool to the temperature of the surroundings. Disregarding radiation or temperature-dependent properties, this time is truly constant, and the typical logarithmic decay results. Since radiation and temperature-dependent properties are included, the time "constants," in fact, depend on temperature and they only approximate the local dynamics. Calculated values of $\tau_{j,\mathrm{HH}}$ are depicted in Fig. 4, indicating that rapid cooling could be achieved with $\tau_o < 10$ s for $T > 425$ °C, and with $\tau_o < 5$ s for $T > 770$ °C. Corresponding heat flow rates are also depicted.

Further, to ensure synchronization between the two domains during numerical simulation, the overall time constant must be made independent of temperature by evaluating it at a certain temperature $\bar{u}$:

$$\tau_o \equiv \tau_o|_{u_i = \bar{u}_i}. \tag{17}$$

Power density is scaled by dividing by $Q^*$, defined as the energy density of the heater, divided by the overall time constant,

$$\tilde{Q} = \frac{Q}{Q^*}, \quad Q^* = \frac{\varrho_{\mathrm{HH}} C_{\mathrm{HH}} u_\infty}{\tau_o}. \tag{18}$$

Downloaded 03 Aug 2007 to 18.33.7.72. Redistribution subject to AIP license or copyright, see http://rsi.aip.org/rsi/copyright.jsp

Thermal resistance is divided by $R^*$, defined as a resistance to heat transport by diffusion $L/(k\times A)$ times the ratio of $\tau_o$ to $\tau_d$,

$$\tilde{R}_i = \frac{R_{\text{thermal}}}{R_i^*}, \quad R^* = \left(\frac{L\tau_o}{kA\tau_d}\right)_i. \tag{19}$$

After scaling of the PDEs and boundary conditions, the following system results:

$$\frac{\partial\tilde{u}_{\text{SB}}}{\partial\tilde{t}} = \frac{\tau_o}{\tau_{d,\text{SB}}}\frac{\partial^2\tilde{u}_{\text{SB}}}{\partial\tilde{x}_{\text{SB}}^2} - \left(\frac{\tau_o}{\tau_{c,\text{SB}}} + \frac{\tau_o}{\tau_{r,\text{SB}}}\right)\tilde{u}_{\text{SB}}, \tag{20}$$

$$\frac{\partial\tilde{u}_{\text{HH}}}{\partial\tilde{t}} = \frac{\tau_o}{\tau_{d,\text{HH}}}\frac{\partial^2\tilde{u}_{\text{HH}}}{\partial\tilde{x}_{\text{HH}}^2} - \left(\frac{\tau_o}{\tau_{c,\text{HH}}} + \frac{\tau_o}{\tau_{r,\text{HH}}}\right)\tilde{u}_{\text{HH}} + \tilde{Q}, \tag{21}$$

and the following boundary conditions apply:

$$\tilde{x}_{\text{SB}} = 0 \rightarrow \frac{A_{\text{SB}}}{S_{\text{SB}}}\left(\frac{\tau_o}{\tau_{c,\text{SB}}} + \frac{\tau_o}{\tau_{r,\text{SB}}}\right)\tilde{u}_{\text{SB}} = \frac{\tau_o}{\tau_{d,\text{SB}}}\frac{\partial\tilde{u}_{\text{SB}}}{\partial\tilde{x}_{\text{SB}}}, \tag{22}$$

$$\tilde{x}_{\text{SB}} = 1 \rightarrow \frac{1}{\tilde{R}_{\text{SB}}}(\tilde{u}_{\text{HH}} - \tilde{u}_{\text{SB}}) = \frac{\tau_o}{\tau_{d,\text{SB}}}\frac{\partial\tilde{u}_{\text{SB}}}{\partial\tilde{x}_{\text{SB}}}, \tag{23}$$

$$\tilde{x}_{\text{HH}} = 0 \rightarrow \frac{\partial\tilde{u}_{\text{HH}}}{\partial\tilde{x}_{\text{HH}}} = 0, \tag{24}$$

$$\tilde{x}_{\text{HH}} = 1 \rightarrow \frac{1}{\tilde{R}_{\text{HH}}}(\tilde{u}_{\text{HH}} - \tilde{u}_{\text{SB}}) = \frac{\tau_o}{\tau_{d,\text{HH}}}\frac{\partial\tilde{u}_{\text{HH}}}{\partial\tilde{x}_{\text{HH}}}. \tag{25}$$

All material properties are temperature dependent and are modeled as such; yet the resistivity of silicon has an especially important effect on the dynamics. Conductivity of silicon is determined by the product of carrier concentration and carrier mobility, and for silicon two regions can be identified. At room temperature the heavily doped silicon is degenerate ("extrinsic range"), and carrier concentration is approximately equal to the impurity concentration. With increasing temperature, carrier mobility decreases due to scattering, resulting in an increase in resistivity. Above the "intrinsic temperature," silicon is nondegenerate ("intrinsic range"), and a strong increase in carrier concentration through thermally activated formation of electron-hole pairs dominates a sharply decreasing resistivity.[19]

Thus, when using a constant current source, dissipated power decreases with increasing temperature, resulting in natural feedback. The influence of local disturbances (e.g., a substrate placed on the heated platform) is reduced by this effect.

### C. Thermal performance

A dynamic input to a suspended heater $(85\times 10\times 0.3\ \text{mm}^3)$ shows its thermal performance, and the measured current is used as input for a simulation to verify the model. Temperature is measured with 75 $\mu$m K-type thermocouples attached to the heater using ceramic adhesive (Ceramabond 865, Aremco), at its center, at 17 mm from the contact block and at 3 mm from the contact block. Measured and simulated temperatures and voltage drops are shown in Figs. 5 and 6. With a geometrically simple model [one dimensional (1D)], considering resistivity and other material properties' dependency on temperature, a very good match between simulation and measurement is achieved. The maximum errors are ≈5% in temperature and ≈2% in voltage.

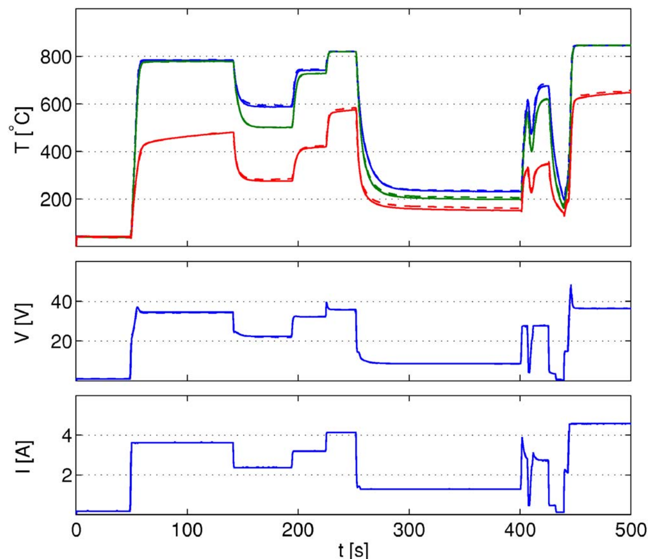


FIG. 5. (Color online) Model validation for a $85\times 10\times 0.3\ \text{mm}^3$ suspended element. Measured current values were used as input for the numerical model. Measured and simulated (dashed graphs) values of voltage drop over the heater and temperature at three locations are shown. Temperature is measured using 75 $\mu$m K-type thermocouples at the center of the heater (top graph), 17 mm from the end (middle graph), and 3 mm from the end (bottom graph).

A heating rate of $dT/dt > 100\ ^\circ\text{C/s}$ is measured, and cooling from $T > 800\ ^\circ\text{C}$ to $T < 600\ ^\circ\text{C}$ (our reaction is stopped below 600 °C) takes ≈5 s. Thus, a thermal cycle between a typical reaction temperature for CNT growth and temperature where the reaction is fully stopped is possible within a period of 7 s, without active cooling.

A stepwise increase of the input current from 0 to 6 A is also simulated, showing increasingly flat temperature profiles

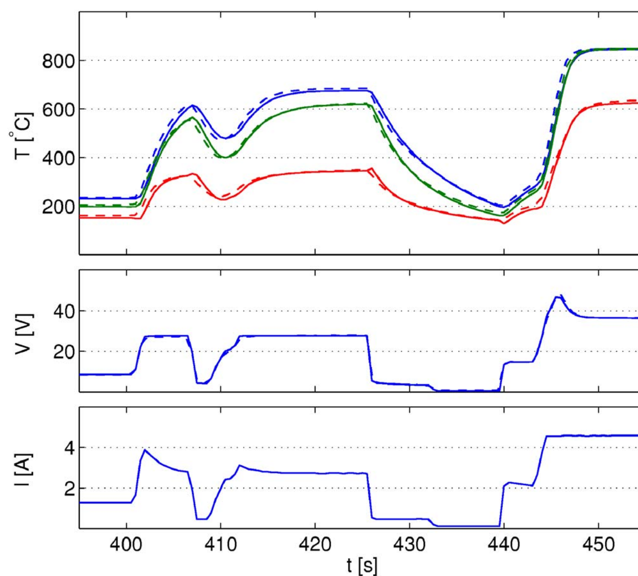


FIG. 6. (Color online) Zoom in at Fig. 5 showing good correspondence, even for highly dynamic input (simulation is dashed line).

Downloaded 03 Aug 2007 to 18.33.7.72. Redistribution subject to AIP license or copyright, see http://rsi.aip.org/rsi/copyright.jsp

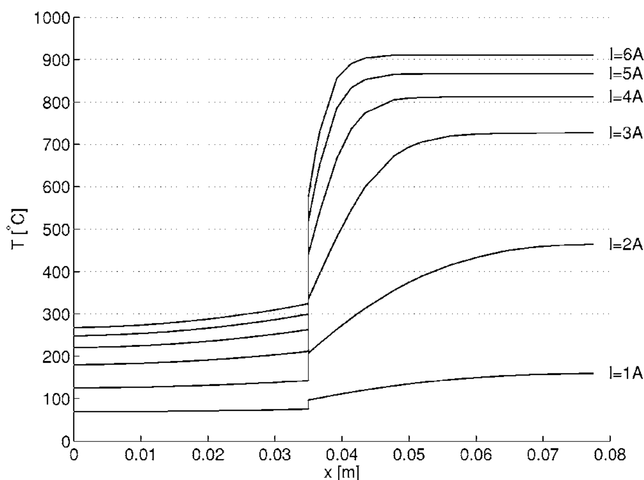


FIG. 7. Simulated steady-state temperature profiles for given input current values. A uniform temperature extends over an increasingly large area of the heater with increasing current.

(Fig. 7). Further, the contact blocks remain below 400 °C, verifying the self-cooling performance.

## III. CVD APPARATUS

### A. Principle of operation and general design aspects

The heated platform and steel blocks are placed inside a quartz tube [48 mm inside diameter (i.d.), 52 mm outside diameter (o.d.), 300 mm length, Finkenbeiner Glass] to provide a controllable gas atmosphere for experiments with surface-bound reactions, such as CVD growth of CNTs. The tube is simply placed on aluminum stands, rendering the heated platform and the growth substrate available for full-field optical observation (Fig. 8).

### B. End caps

The quartz tube is sealed with end caps, which feature Viton lip seals (Chicago Rawhide) recessed in grooves in a turned aluminum piece (standard 6061 alloy), as shown in Fig. 9. Commonly used end caps with face seals can be cumbersome to align; the new design easily slides over the end of the tube and self-aligns. The seals are spaced to impart sufficient pitch stiffness when the seals soften upon heating; yet the radial compliance of the seals results in a low-stress connection. The initial fit preloads the seals and increased pressure further engages the seals, employing the principle of self-help.[20] The end caps seal against overpressure up to ≈30 kPa but slide off if pressure is increased further, thus protecting against possibly dangerous overpressure in the case of an accidental ignition of the reaction gases or a clogged gas exit line. The hoop stress in the quartz tube wall,

$$\sigma_h = (p \times r)/t_w = 6 \times p, \tag{26}$$

remains far below the modulus of rupture of fused quartz, $\sigma_h \leqslant 60$ MPa.[21]

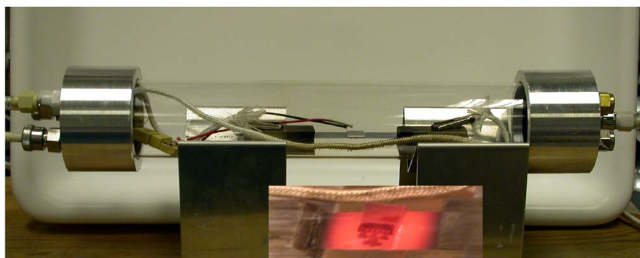

FIG. 8. (Color online) Prototype "platform-in-tube" reactor apparatus, where suspended heated platform is mounted on stainless steel contact electrodes and sealed inside horizontal quartz tube. Inset shows oblique view of platform at 825 °C, with VA-CNT microstructures growing from lithographically patterned catalyst film.

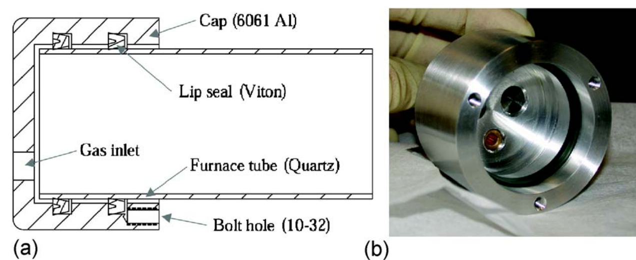


FIG. 9. (Color online) Elastokinematically constrained furnace tube end caps using lip seals: (a) Cross-section drawing showing Viton seals recessed in grooved aluminum and (b) cap seal for 46 mm o.d. quartz tube, with one lip seal.

### C. Gas supply

For CNT growth, gases are supplied to the quartz tube via manual needle-valve rotameters (Gilmont, Matheson Tri-Gas). One rotameter is used for each line of $CH_4$ (99.995%, BOC), $C_2H_4$ (99.5%, Airgas), $H_2$ (99.999%, Airgas), and Ar (99.999%, Airgas). The output lines of the rotameters join at a manifold, and the gas mixture is fed to the quartz tube through a four-bore ceramic pipe (6.35 mm o.d., 1.8 mm bore i.d., 99.8% purity $Al_2O_3$, Omega). The delivery pipe is held in a Cajon-type (Swagelok Ultra-Torr) fitting in one of the end caps.

The exhaust gas passes through a bubbler that provides a constant backpressure to stabilize the flow inside the tube. Therefore, the pressure in the apparatus is ≈0.1 psi above atmospheric, as established by the oil level in the bubbler.

In this configuration, the reaction gases are first heated upon contact with the heated platform. In an alternative setup, gases are preheated while passing through the delivery pipe. For this purpose, a resistance wire of ≈10 Ω is wrapped around the pipe over a distance of 75 mm and 30 V is applied to heat the wire.

## IV. EXPERIMENT: CVD GROWTH OF CNTs

We demonstrate growth of both tangled films of single wall CNTs (SWCNTs) (process 1,[13]) and vertically aligned films of multi wall CNTs (MWCNTs) (process 2,[14]) on the heated platform, using CVD reactions which we previously developed using a conventional tube furnace. To start, a piece of silicon wafer (≈10 mm × 10 mm × 600 μm thickness) coated with a catalyst film deposited by electron beam evaporation (3.0/1.5/20 nm Mo/Fe/$Al_2O_3$ for SWCNT growth, and 1/10 nm Fe/$Al_2O_3$ for MWCNT growth) is rested on the center of the heated platform. The platform assembly is placed inside the quartz tube, and the end caps

Downloaded 03 Aug 2007 to 18.33.7.72. Redistribution subject to AIP license or copyright, see http://rsi.aip.org/rsi/copyright.jsp

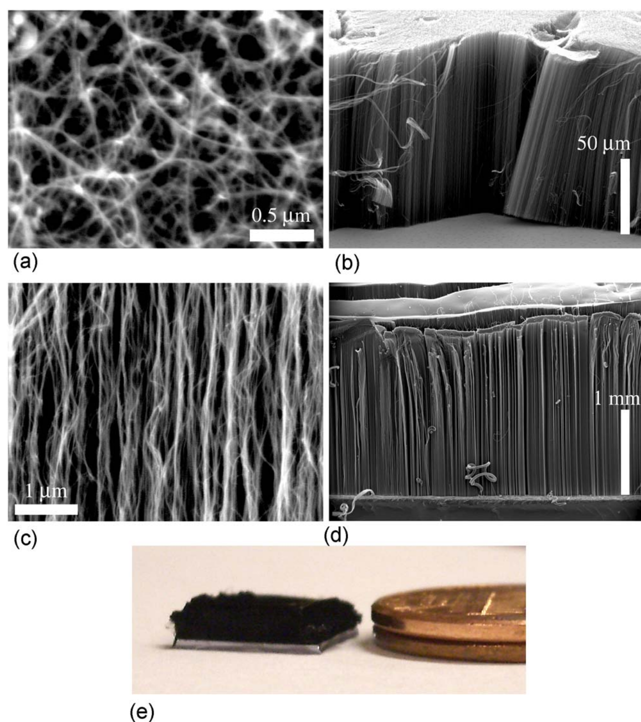


FIG. 10. (Color online) CNT films grown from catalyst-coated silicon substrates rested on the resistively heated platform: (a) Tangled SWCNT film, grown from $Mo/Fe/Al_2O_3$ catalyst film in $CH_4/H_2$; (b) ≈0.1 mm thick VA-CNT film, grown from $Fe/Al_2O_3$ film in $C_2H_4/H_2/Ar$; (c) alignment of CNTs within film shown in (b); (d) ≈2 mm thick VA-CNT film, grown as in (b) with pretreatment by flowing gas through heated $Al_2O_3$ delivery pipe; and (e) optical image of film on silicon substrate, placed next to two stacked United States pennies (each 1.42 mm thick).

are mounted to seal the atmosphere. Next, the tube is flushed with 600 SCCM Ar for 10 min, and then the platform is heated by stepping the power supply to a preset value. After 2 min, the flow into the tube is adjusted to $H_2/Ar$ (2 min at 200/200 SCCM $H_2/Ar$ for process 1; 5 min at 400/140 SCCM $H_2/Ar$ for process 2). Then, the flow is adjusted to include the carbon source (800/200 SCCM $CH_4/H_2$ for process 1; 115/400/140 SCCM $C_2H_4/H_2/Ar$ for process 2) and maintained for a typical growth period of 15 min, during which the supply current is held constant.

Using the heated platform, process 1 yields a dense film of tangled CNTs, as shown in Fig. 10(a). Using Raman spectroscopy and transmission electron microscopy (results not shown), these are confirmed to be primarily SWCNTs. Alternatively, process 2 yields a film of vertically aligned CNTs [Fig. 10(b)], which are shown to be MWCNTs (≈10 nm o.d.). In process 1, the SWCNTs begin growing at a relatively low areal density on the substrate and quickly become entangled due to surface interactions among the CNTs and the substrate. This hindrance limits the film thickness to ≈1 $\mu$m. In process 2, the CNTs grow at a higher areal density and self-orient perpendicular to the substrate surface due to initial crowding.[22,23] This vertically aligned [Fig. 10(c)] conformation enables the CNT film to grow to millimeter-scale thickness.

However, the vertically aligned (VA)-MWCNT film grown using process 2 with the heated platform is only 0.1 mm thick, compared to ≈1 mm thickness which is routinely obtained by growth in the conventional tube furnace. This implies that thermal decomposition of the reactant mixture significantly affects its chemical activity for CNT growth. When the gas flows through a heated tube before reaching the substrate, gas-phase reactions form additional species [e.g., $C_2H_4$ homogeneously reforms into $C_2H_2$, $CH_4$, $C_2H_6$, $C_3H_6$, $C_3H_8$, $C_4H_4$, $C_4H_6$, and $H_2$ (Ref. 24)] which contribute significantly to the growth reaction. Alternatively, when only the growth substrate is heated there is less time for thermal decomposition of the reactants prior to reaching the catalyst.

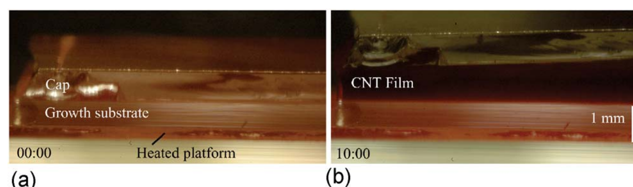


FIG. 11. (Color online) Optical imaging of VA-CNT film growth on the suspended heated platform, with platform at 825 °C: (a) Side view showing initial configuration, where "cap" substrate is placed on top of growth substrate to moderate gas flow and to serve as an optical reference and (b) snapshot after 10 min of reaction, where the film thickness exceeds 1 mm.

To qualitatively study this effect, we next replicated process 2 while first flowing the reactant through the heated delivery pipe. In this case, the film grows to ≈2.0 mm in 15 min [Fig. 10(d)], roughly doubling the growth rate obtained in the tube furnace. We attribute this increase to thermal decomposition of the reactant when it is rapidly heated to ≈1000 °C, which exceeds the temperature of 750 °C reached in the tube furnace and is also above the self-pyrolysis temperature of $C_2H_4$. However, the brief residence time in the heated pipe prevents excessive sooting. Further, the gas cools as it exits the heated pipe before it reaches the heated platform, suggesting that the thermal "pretreatment" step creates more reactive species rather than unstable radicals.

## V. DISCUSSION

Although much further study is needed, the heated platform system is a useful new instrument for decoupling the temperature of reactant pretreatment from the temperature of the reaction surface. Our preliminary results suggest that independent control of these temperatures can improve the efficiency of CNT growth. Going forward, *in situ* optical interrogation of the CNTs on the reaction surface (e.g., laser measurement of film thickness) can be combined with gas analysis (e.g., mass spectrometry) to directly relate the reaction kinetics to the chemical nature of the reactant. As a first example of optical reaction diagnosis using the heated platform apparatus, we imaged VA-CNT film growth by focusing a digital still camera (Nikon) on the platform mounted inside the quartz tube. We can monitor the thickness of the film versus time by mounting the camera in a side-view configuration (Fig. 11).

Overall, the suspended heated platform is a versatile and low-cost reaction apparatus which can be used for a range of laboratory-scale duties ranging from simple CVD studies to detailed *in situ* investigations of reaction progress enabled by

Downloaded 03 Aug 2007 to 18.33.7.72. Redistribution subject to AIP license or copyright, see http://rsi.aip.org/rsi/copyright.jsp

its "open" design. The capability for rapid temperature adjustment without active cooling enables new studies of reactions under dynamic thermal control. An analytical one-dimensional model accurately describes the thermal behavior of the suspended platform, which is dominated by the temperature-dependent resistivity of silicon. This model and design principle can be extended to other heater substrates such as graphite, conductive ceramics, and metal foils; however, silicon is found to be especially useful because a centimeter-scale element can be heated to $\approx 1000\,^{\circ}\mathrm{C}$ using a simple benchtop power supply. The model can be scaled to accurately predict the thermal performance of heaters of different sizes and geometries; for example, we can simulate the addition of a second substrate at the center of the platform (representing a heated sample), or variation of the cross-sectional dimensions of the platform along its length, as long as the assumption of no transverse gradients holds. For relatively wide or thick substrates, the model should be expanded to two dimensional (2D) or three dimensional (3D), in which case final element analysis will prove more effective.

We have used a simple first-generation apparatus to study growth of CNT films using CVD of hydrocarbon gases on silicon substrates coated with transition metal catalyst films. We have replicated processes for growth of tangled SWCNT and aligned MWCNT films which we previously developed using traditional externally heated tube furnaces. This investigation has led to a qualitative understanding of the importance of thermal decomposition on the activity of gaseous reactants for CNT growth. The localization of heating at the suspended platform is enabling further study by independent thermal pretreatment of the reaction gases, coupled with real-time optical characterization of the film growth kinetics. Going forward, the suspended platform apparatus could be used to study a wide variety of surface reactions including growth of semiconducting nanowires and catalytic reforming of gas streams. It can also serve as a simple benchtop apparatus for thermal control of microreactors and for rapid thermal processing of thin films and semiconductor and micromechanical devices.

## ACKNOWLEDGMENTS

This work was funded by NSF Grant No. DMI-0521985 and by an Ignition Grant from the MIT Deshpande Center for Technological Innovation. One of the authors (A.J.H.) is grateful for a Fannie and John Hertz Foundation Fellowship. The authors thank M. P. Brenner of Harvard University for discussions regarding the thermal model.

## NOMENCLATURE

$\epsilon$ = emissivity (dimensionless)
$\rho$ = resistivity ($\Omega$ m)
$\phi$ = heat flux ($\mathrm{W/m^2}$)
$\varrho$ = mass density ($\mathrm{kg/m^3}$)
$\sigma$ = Stefan-Boltzmann constant $=5.67\times 10^{-8}\,[\mathrm{W/(m^2\,K^4)}]$
$\tau_o$ = overall time constant (s), see Eq. (12)
$\tau_d$ = time constant for diffusion (s), see Eq. (14)
$\tau_c$ = time constant for convection (s), see Eq. (15)
$\tau_r$ = time constant for radiation (s), see Eq. (16)
$A$ = cross-sectional area ($\mathrm{m^2}$)
$C$ = heat capacity [J/(kg K)]
$I$ = current (A)
$L$ = length (m)
Nu = Nusselt number (dimensionless)
$P$ = perimeter (m)
$Q$ = dissipated power density ($\mathrm{W/m^3}$)
$Q^*$ = scaling factor for dissipated power density, see Eq. (18)
$R_{\mathrm{thermal}}$ = thermal resistance (K/W)
$R^*$ = scaling factor for thermal resistance, see Eq. (19)
$S$ = surface area ($\mathrm{m^2}$)
$T$ = temperature (°C)
$V$ = volume ($\mathrm{m^3}$)
$h$ = convection heat transfer coefficient $[\mathrm{W/(m^2\,K)}]$
$k$ = thermal conductivity [W/(m K)]
$p$ = pressure (Pa)
$r$ = internal radius (m)
$t$ = time (s)
$t_w$ = wall thickness (m)
$u$ = temperature (K)
$u_\infty$ = temperature of surroundings (K)
$u_{\mathrm{SB}}^-$ = temperature at contact on steel block side
$u_{\mathrm{SB}}^+$ = temperature at contact on half heater side
$w$ = heat loss to surroundings $[\mathrm{W/(m^2)}]$
$x$ = position (m)
$\tilde{}$ = scaled variable, for example $\tilde{t}$
$i$ = domain index (SB or HH)
SB = steel block
HH = half heater

[1] H. A. Hansen, J. L. Olsen, S. Jensen, O. Hansen, and U. J. Quaade, Catal. Commun. **7**, 272 (2006).
[2] Y. L. Li, I. A. Kinloch, M. S. P. Shaffer, C. Singh, J. F. Geng, B. F. G. Johnson, and A. H. Windle, Chem. Mater. **16**, 5637 (2004).
[3] J. J. Brandner, G. Emig, M. A. Liauw, and K. Schubert, Chem. Eng. J. **101**, 217 (2004).
[4] S. M. Huang, M. Woodson, R. Smalley, and J. Liu, Nano Lett. **4**, 1025 (2004).
[5] K. Thompson, Y. B. Gianchandani, J. Booske, and R. F. Cooper, J. Microelectromech. Syst. **11**, 285 (2002).
[6] E. H. Hong, K. H. Lee, S. H. Oh, and C. G. Park, Adv. Mater. (Weinheim, Ger.) **14**, 676 (2002).
[7] B. J. Yoon *et al.*, J. Am. Chem. Soc. **127**, 8234 (2005).
[8] Y. Kim, I. Choi, S. K. Kang, J. Lee, and J. Yi, Rev. Sci. Instrum. **77**, 1 (2006).
[9] M. L. Trawick, D. E. Angelescu, and P. M. Chaikin, Rev. Sci. Instrum. **74**, 1390 (2003).
[10] G. Kolb and V. Hessel, Chem. Eng. J. **98**, 1 (2004).
[11] R. H. Baughman, A. A. Zakhidov, and W. A. de Heer, Science **297**, 787 (2002).
[12] M. Endo, T. Hayashi, Y. A. Kim, M. Terrones, and M. S. Dresselhaus, Philos. Trans. R. Soc. London, Ser. A **362**, 2223 (2004).
[13] A. J. Hart, A. H. Slocum, and L. Royer, Carbon **44**, 348 (2006).
[14] A. J. Hart and A. H. Slocum, J. Phys. Chem. B **110**, 8250 (2006).
[15] J. Tauc, *Photo and Thermoelectric Effects in Semiconductors*, International Series of Monographs on Semiconductors Vol. 2 (Pergamon, Oxford, 1962).
[16] CINDAS, Thermophysical properties of matter database (https://cindasdata.com/) 2003–2005.
[17] F. P. Incropera and D. P. DeWitt, *Introduction to Heat Transfer*, 3rd ed.

Downloaded 03 Aug 2007 to 18.33.7.72. Redistribution subject to AIP license or copyright, see http://rsi.aip.org/rsi/copyright.jsp

(Wiley, New York, 1996).
[18] R. Haberman, *Elementary Applied Partial Differential Equations: With Fourier Series and Boundary Value Problems*, 3rd ed. (Prentice-Hall, Upper Saddle River, NJ, 1998).
[19] J. Bardeen and G. L. Pearson, Phys. Rev. **75**, 865 (1949).
[20] A. H. Slocum, *Precision Machine Design* (Society of Manufacturing Engineers, Dearborn, MI, 1992).
[21] G. Finkenbeiner Inc. Website (http://www.finkenbeiner.com/), 2006.
[22] M. Terrones *et al.*, Nature (London) **388**, 52 (1997).
[23] S. S. Fan, M. G. Chapline, N. R. Franklin, T. W. Tombler, A. M. Cassell, and H. J. Dai, Science **283**, 512 (1999).
[24] G. D. Towell and J. J. Martin, AIChE J. **7**, 693 (1961).

Downloaded 03 Aug 2007 to 18.33.7.72. Redistribution subject to AIP license or copyright, see http://rsi.aip.org/rsi/copyright.jsp